communications biology

ARTICLE

https://doi.org/10.1038/s42003-021-01979-5 OPEN

Multinucleation associated DNA damage blocks proliferation in p53-compromised cells

Madeleine Hart[1], Sophie D. Adams[1] & Viji M. Draviam[1✉]

Nuclear atypia is one of the hallmarks of cancers. Here, we perform single-cell tracking studies to determine the immediate and long-term impact of nuclear atypia. Tracking the fate of newborn cells exhibiting nuclear atypia shows that multinucleation, unlike other forms of nuclear atypia, blocks proliferation in p53-compromised cells. Because ~50% of cancers display compromised p53, we explored how multinucleation blocks proliferation. Multinucleation increases 53BP1-decorated nuclear bodies (DNA damage repair platforms), along with a heterogeneous reduction in transcription and protein accumulation across the multinucleated compartments. Multinucleation Associated DNA Damage associated with 53BP1-bodies remains unresolved for days, despite an intact NHEJ machinery that repairs laser-induced DNA damage within minutes. Persistent DNA damage, a DNA replication block, and reduced phospho-Rb, reveal a novel replication stress independent cell cycle arrest caused by mitotic lesions. These findings call for segregating protective and prohibitive nuclear atypia to inform therapeutic approaches aimed at limiting tumour heterogeneity.

[1] School of Biological and Chemical Sciences, Queen Mary University of London, London, UK. ✉email: v.draviam@qmul.ac.uk

Nuclear atypia is associated with disease states, and is a strong discriminator of survival in many cancers[1,2]. Micronuclei, a form of nuclear atypia, harbour nuclear envelope defects[3], leading to cell cycle asynchronicity between the micro- and primary nuclei[4] and extensive DNA damage following replication stress[4,5]. Furthermore, the erroneous repair of the micronuclear DNA[5,6] promotes large scale translocations confined to micronuclear DNA[5]. Thus, micronuclei can propagate genomic instability and therefore, can be considered tumourigenic, particularly given their ability to proliferate in p53 null conditions[4,7]. While micronuclei studies provide evidence that nuclear atypia may be causal to a disease state, what impact other forms of nuclear atypia have upon a disease state is largely unknown.

Multinucleation, another form of nuclear atypia with multiple nuclear compartments, has been linked to mitotic slippage[8] the erroneous exit from a prolonged mitotic arrest. Whilst multinucleated cells are known to display DNA damage[8–10], their cell cycle fate compared to those of micronucleated cells and the dynamics of DNA damage and downstream signalling have not been assessed.

Dormant giant multinucleated cells are a hallmark of metastasis and disease relapse following anticancer treatment (reviewed in[11]). In over 50% of aggressive cancers, p53 function is compromised[12] either through mutations or oncoprotein expression[13,14]. Whether and how multinucleated cells proliferate in p53 compromised tissues is not known. Downstream of p53, p21 inhibits CDK activity and reduces phospho-Rb levels which blocks cells at the restriction point and promotes quiescence[15,16]. Absence of Rb phosphorylation (Ser 807/811) has been used to infer reduced CDK2 activity and as a marker of quiescence[17–22]. Understanding whether distinct mitotic errors affect pRb status differently will provide insight into how multinucleated cells thrive in aggressive cancer tissues.

Mitotic errors can lead to a variety of nuclear atypia, including micronucleation, multinucleation or misshapen nuclei, arising either as a result of mitotic slippage (slow exit) or spindle checkpoint failure (abrupt exit) (reviewed in[23]). While structural aneuploidies can impair cell cycle progression[24], the cell cycle impact of various nuclear atypia has not been compared so far within a common mitotic lesion. A molecular understanding how nuclear atypia impacts cell viability and DNA repair status in single-cells of a population is important to understand disease outcome heterogeneity.

To investigate how distinct forms of nuclear atypia differently impact cell fate, we performed single-cell tracking studies to investigate the impact of mitotic lesions on nuclear compartments and cell proliferation. Quantitative analysis of cell fate showed a significant difference between multinucleation and micronucleation, a catastrophic nuclear atypia known to promote genomic rearrangements and tumour heterogeneity. Multinucleation, unlike other forms of nuclear atypia, blocks proliferation in p53-compromised cells. Multinucleation increases 53BP1-decorated nuclear bodies (DNA damage repair platforms), along with a heterogeneous reduction in transcription and protein accumulation across the multi-nucleated compartments. Importantly, 53BP1- bodies at the sites of Multinucleation Associated DNA Damage (MADD) remain unresolved for days, despite an intact NHEJ machinery that repairs laser-induced DNA damage within minutes. We propose that the persistent MADD signalling blocks the onset of DNA replication and is associated with driving proliferative cells into a low phospho-Rb quiescent state, revealing a protective proliferation block, despite compromised p53, in multinucleated cells.

Results

Unlike other nuclear atypia, multinucleation induces a G1 arrest despite compromised p53. To mimic mitotic drug treatment associated nuclear atypia, we exposed cells to GSK-923295, a CENP-E inhibitor (CENPEi), which disrupts the end-on conversion of chromosome-microtubule attachment[25,26] leading to chromosome misalignment and a mitotic arrest[27] causing mitotic slippage and a variety of nuclear atypia. To analyse cell cycle status, we immunostained for PCNA foci (S-phase marker) two days after the release from CENPEi treatment (Fig. 1a). Using immunostaining we compared 100 s of RPE1 cells displaying a variety of nuclear atypia. As expected, multinucleation, micronucleation or misshapen nuclei were all observed predominantly in the CENPEi-treated but not DMSO-treated population (Fig. 1b, c). Only in cells displaying multinucleation, no PCNA foci was observed; cells displaying micronuclei or normal or misshapen nuclei presented a small proportion of PCNA foci positive cells (Fig. 1b, d), showing a multinucleation associated block in G1-S transition and replication initiation.

The complete absence of PCNA foci in multinucleated cells is somewhat at odds with reports of a positive association between multinucleation and tumorigenic potential and resistance to therapy[11,28]. So, we investigated whether the G1-S block in multinucleated cells may be lost following compromised p53 function, a tumour suppressor frequently lost in cancers (reviewed by[29]). A p53 dependent G1-S block has been reported in micronucleated cells[7], tetraploid cells[30] and chromosomal missegregation or aneuploidy[7,31,32], but not tested in multinucleated cells. We exposed RPE1 p53 knockdown cell line, with demonstrably no p53 expression[7] (Supplementary Fig. 1a, b and 7a) to CENP-E inhibitor and monitored PCNA status 48 h after inhibitor wash-off (Fig. 1a). In p53 knockdown cells, where all three forms of nuclear atypia could be observed (Fig. 1f), nuclear PCNA foci, distinctly brighter than non-specific cytoplasmic speckles, were absent in multinucleated cells alone (Fig. 1e, g). In contrast, cells presenting other nuclear atypia, including micronucleated or misshapen nuclei showed an increase in the proportion of PCNA foci in p53 knockdown cells compared to WT RPE1 cells (Fig. 1e, g). The lack of PCNA foci selectively in multinucleated cells shows that unlike other forms of nuclear atypia, multinucleation disallows S-phase entry, independent of p53 status.

Two other mitotic lesions where multinucleation is not readily induced due to accelerated mitotic exit, inhibitions of MPS1 or Aurora-B activity, yielded similar results (Supplementary Fig. 2a, b). Assessing the cell cycle impact of micronuclei and misshapen nuclei showed that in p53 WT conditions both treatments exhibit a G1 arrest, but less robust than multinucleate cells (Supplementary Fig. 2c). In addition, in p53 knockdown cells, the G1 arrest was alleviated in micronucleated and misshapen nuclei caused following MPS1 or Aurora-B inhibition (Supplementary Fig. 2d-f). In summary, unlike other nuclear atypia, multinucleation uniquely blocks G1 despite a compromised p53 status.

Multinucleate cells exhibit the highest incidence of DNA damage. We compared the extent of DNA damage in the various nuclear atypia, by immunostaining for gamma H2AX (double-stranded DNA damage marker), 1 and 48 h after CENPEi washout. 48 h after washout, 40% of micronuclei bearing cells displayed gH2AX foci exclusively within the micronuclei compartment, as reported[4,5,33] and only 30% of their primary nuclei presented gH2AX foci (Supplementary Fig. 3a, b). In contrast, >90% of multinucleated cells displayed gH2AX foci in most of the compartments (Supplementary Fig. 3a, b). Importantly, the number of gH2AX foci is strikingly higher after multinucleation compared to other forms of nuclear atypia (Supplementary Fig. 3c), although the intensity of individual gH2AX foci per se was not different (Supplementary Fig. 3d). Similarly, within an hour of drug washout, gH2AX foci number was strikingly higher

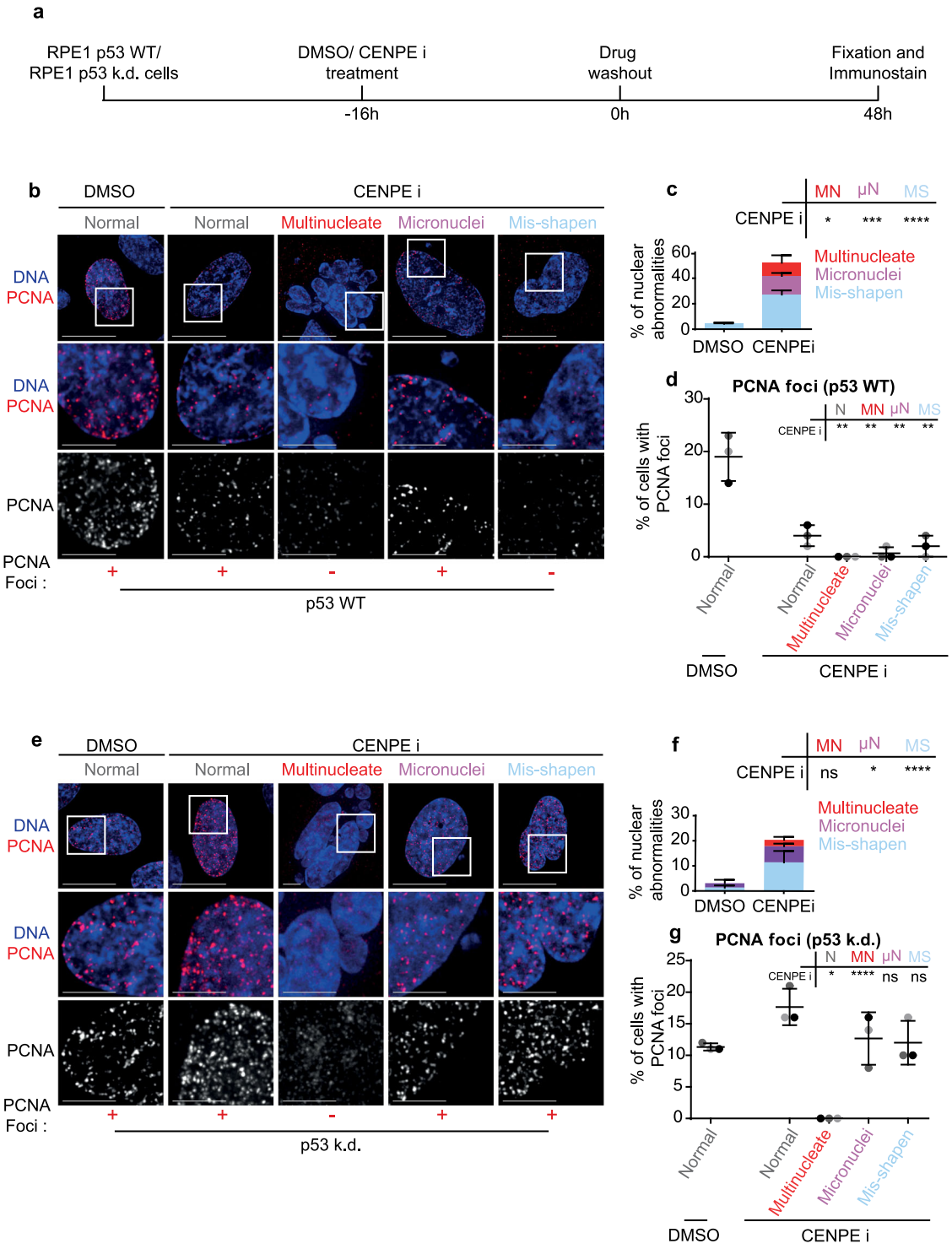

Fig. 1 Unlike other nuclear atypia, multinucleation induces a G1 arrest, independent of p53. a Experimental regime; RPE1 p53 wild type (WT) or RPE1 p53 knockdown (k.d.) were treated with DMSO or CENPE inhibitor for 16 h, then washed out. 48 h later cells were assessed for PCNA and nuclear status. Images of RPE1 p53 WT (**b**) or p53 k.d (**e**) cells treated as in a. Scale 15 µm, insets 5 µm. ± refers to PCNA foci positive or negative nuclei displayed. In Fig. 1b, a micronuclei bearing cell displaying PCNA-foci has been chosen, although the majority lack PCNA-foci. Quantification of nuclear morphology changes after treatment of RPE1 p53 WT (**c**) or p53 k.d (**f**) cells with DMSO or CENPE inhibitor, as in (**a**). Nuclei were classified as either Mis-shapen (MS), Micronucleated (µN) or Multinucleated (MN). $N = 600$ cells, 3 independent experimental repeats shown as shades of grey. Statistical analysis was using a two-way ANOVA with multiple comparisons and a confidence interval of 95%. **d**, **g** Quantification of the percentage of PCNA-foci positive cells, within each nuclear morphology bin, following DMSO or CENPE inhibitor treatment, of RPE1 p53 WT (**c**) or p53 k.d (**f**) cells. $N > 150$, 3 independent experimental repeats shown as shades of grey. Statistical analysis was using multiple unpaired *t* tests, comparing each morphology after CENPE inhibition to normal nuclei after DMSO treatment.

in multinucleated cells (Supplementary Fig. 4, see 4e). These observations show that multinucleated cells are prone to a substantially higher incidence of DNA damage compared to other forms of nuclear atypia.

Next, we analysed the incidence of RIF1, an NHEJ repair pathway member that accumulates at DNA breaks specifically in G1 phase[34–36]. Immunostaining studies showed the normal accumulation of RIF1 in the vast majority of gH2AX foci in multinucleated cells, except for the gH2AX foci in micronucleated compartments (Supplementary Fig. 3e). We conclude that Multinucleation associated DNA damage (MADD) successfully accumulates RIF1, a factor that promotes NHEJ in the G1 phase of cell cycle.

Multinucleate cells exhibit delayed DNA damage signalling. To identify the precise timing of MADD and the extent of MADD resolution, we used time-lapse microscopy to track the arrival and departure of 53BP1 foci, a DNA damage response factor downstream of gH2AX and upstream of RIF1. In RPE1 cells coexpressing 53BP1-GFP and Histone-2B-GFP (DNA marker), we performed long-term live-cell imaging for at least more than 10 h[37] to compare multinucleated cells arising from a slow mitotic slippage or rapid mitotic exit following either CENP-Ei treatment alone or CENP-Ei and Aurora-Bi co-treatment, respectively (Supplementary Fig. 5a; Fig. 2a, b; Supplementary Videos 1a–c). Videos of CENPEi washout cell cultures showed nearly 80% of cells exiting mitosis with a multinucleate phenotype and only 20% of cells exhibiting either a normal or misshapen nuclei (Supplementary Fig. 5b). 53BP1 foci could be observed in multinucleated cells, as well as those with normal or misshapen nuclei (Fig. 2c), consistent with gH2AX status (Supplementary Fig. 4), with multinucleated cells gaining foci in ~60% of cells during the course of imaging irrespective of slow mitotic slippage (CenpEi) or a rapid mitotic exit (CenpEi & AuroraBi). Analysis of live-cell videos revealed that the timing of 53BP1 foci arrival varies depending on the nuclear atypia: in multinucleated cells, 53BP1 foci arrival is delayed, ~2–11 h after mitotic exit (Fig. 2d), whereas in others foci arrival was complete, within the first 4 h after mitotic exit (Fig. 2d). In fixed-cell studies, gH2AX foci (Supplementary Fig. 4) appear within 1 h following drug washout, showing a delayed 53BP1 response in multinucleated cells.

In all multinucleated cells, irrespective of slow mitotic slippage or rapid mitotic exit, 53BP1 foci resolution was lacking and the foci number was steadily increasing in late G1 (Supplementary Fig. 5c, Fig. 2e). These single-cell tracking studies reveal that while none of the multinucleated cells resolved 53BP1 foci completely ($n = 55$), 40–50% of normal nuclei displayed 53BP1 foci disappearance indicative of damage clearance ($n = 8$ DMSO and 9 CENPEi cells) (Supplementary Fig. 5c). We conclude that MADD signalling is delayed and MADD remains unresolved.

MADD-associated 53BP1 remains unresolved despite intact DDR in multinucleated cells. We investigated whether MADD can not be resolved or multinucleated cells are DNA Damage Repair (DDR) deficient by tracking the fate of laser-induced DNA damage in 53BP1-GFP expressing multinucleated cells. Comparing images before and after laser-induced damage showed that cells displaying multinucleation or normal nuclei can rapidly recruit 53BP1-GFP at the laser-damage site (Fig. 3a). The acquisition of laser-induced 53BP1-GFP foci was slightly reduced in number and delayed in multinucleated cells compared to normal cells (Fig. 3b, c). Clearance of laser-induced 53BP1 foci was surprisingly slightly more frequent in multinucleated cells compared to normal cells (Fig. 3d). Comparing the rates of laser-induced 53BP1 foci clearance showed no difference between a multinucleated versus normal cell (Fig. 3e, f), revealing a proficient DDR pathway in multinucleated cells. Despite DDR proficiency, multinucleated cells did not resolve any of the non-laser induced 53BP1 foci, while normal nuclei resolved 40% of the foci during imaging of up to 15 h (Fig. 3e). These data show that MADD associated 53BP1 foci cannot be resolved despite a proficient DDR response in multinucleated cells.

Multinucleation blocks proliferation despite compromised p53. Tracking the impact of multinucleation on cell cycle progression, using time-lapse microscopy, revealed an important heterogeneity across multinucleate compartments. In non-transformed hTERT-RPE1 cells expressing mRuby-PCNA (S-phase Marker) and p21-GFP (G1-phase marker), normal nuclei in both CENP-Ei or DMSO treated conditions showed normal appearance and disappearance of PCNA foci (CENP-Ei = 71; DMSO = 195 cells; Supplementary Videos 2a and b; Fig. 4a, b). In contrast, cells displaying multinucleation showed no PCNA foci formation for at least 14 h after mitosis, despite the accumulation of nuclear mRuby-PCNA levels in most compartments (114 Cells; Supplementary Video 2c; Fig. 4b). Consistent with the lack of PCNA foci, multinucleated cells showed an increase in nuclear p21-GFP, 4–5 h after mitotic exit (Fig. 4b, c). Increasing p21-GFP signal was observed in multinucleated cells despite its absence at mitotic exit (Supplementary Video 2c, Fig. 4b), indicating a stress signalling response in late G1. Importantly, a variable increase in the rates and amount of p21 accumulation across different compartments of multinucleated cells was observed (Fig. 4c; $n = 3$ cells). In summary, multinucleation promotes a steady increase in nuclear p21, heterogeneously across compartments, disallowing the onset of DNA replication.

We hypothesised that if multinucleated cells are not dead and multinucleation disrupts genome-wide function, we should see signs of altered transcription, and we were curious to see if the transcription can occur at MADD-sites. To test whether MADD heterogeneously prevents the function of transcriptional machinery, we immunostained using antibodies against gH2AX and either RNA-Pol II pSer5 (initiation marker) or RNA-Pol II pSer2 (elongation marker). Both markers were present irrespective of nuclear atypia (Fig. 4d; Supplementary Fig. 6c) showing the ability to localise transcriptional machinery and phosphorylate key sites to enable transcriptional initiation and elongation despite large-scale fragmentation of nuclear compartments in multinucleated cells. However, transcription-associated foci did not overlap with gH2AX demonstrating a shutdown of transcription proximal to MADD sites (Fig. 4d; Supplementary Fig. 6c), similar to transcription exclusion at 53BP1 foci arising from replication stress[38].

Quantifying RNA-Pol II pSer5 or pSer2 foci intensities in nuclei or within a nuclear compartment revealed a statistically significant decrease in mean intensities in some compartments of both multinucleated and micronucleated cells (Fig. 4e; Supplementary Fig. 6d). To investigate whether RNA-Pol intensities are dependent on nuclear compartment size, we correlated changes in mean intensity and compartment size. Micronucleated cells had reduced mean intensities in micronuclei but not primary nuclei, while the compartments in multinucleated cells displayed a unique heterogenous spread of intensities (Fig. 4f; Supplementary Fig. 6e). We tested whether reduced RNA-Pol intensities reflect a reduction in RNA-Pol at each transcriptional site or due to a reduction in the number of transcriptional sites. The proportion of nucleus occupied by RNA-Pol pSer5 or pSer2 foci was reduced in micronucleated and some smaller compartments of multinucleated cells (Supplementary Fig. 6a, f). In smaller multinucleate compartments (<40 um^2) a transcriptional variability is

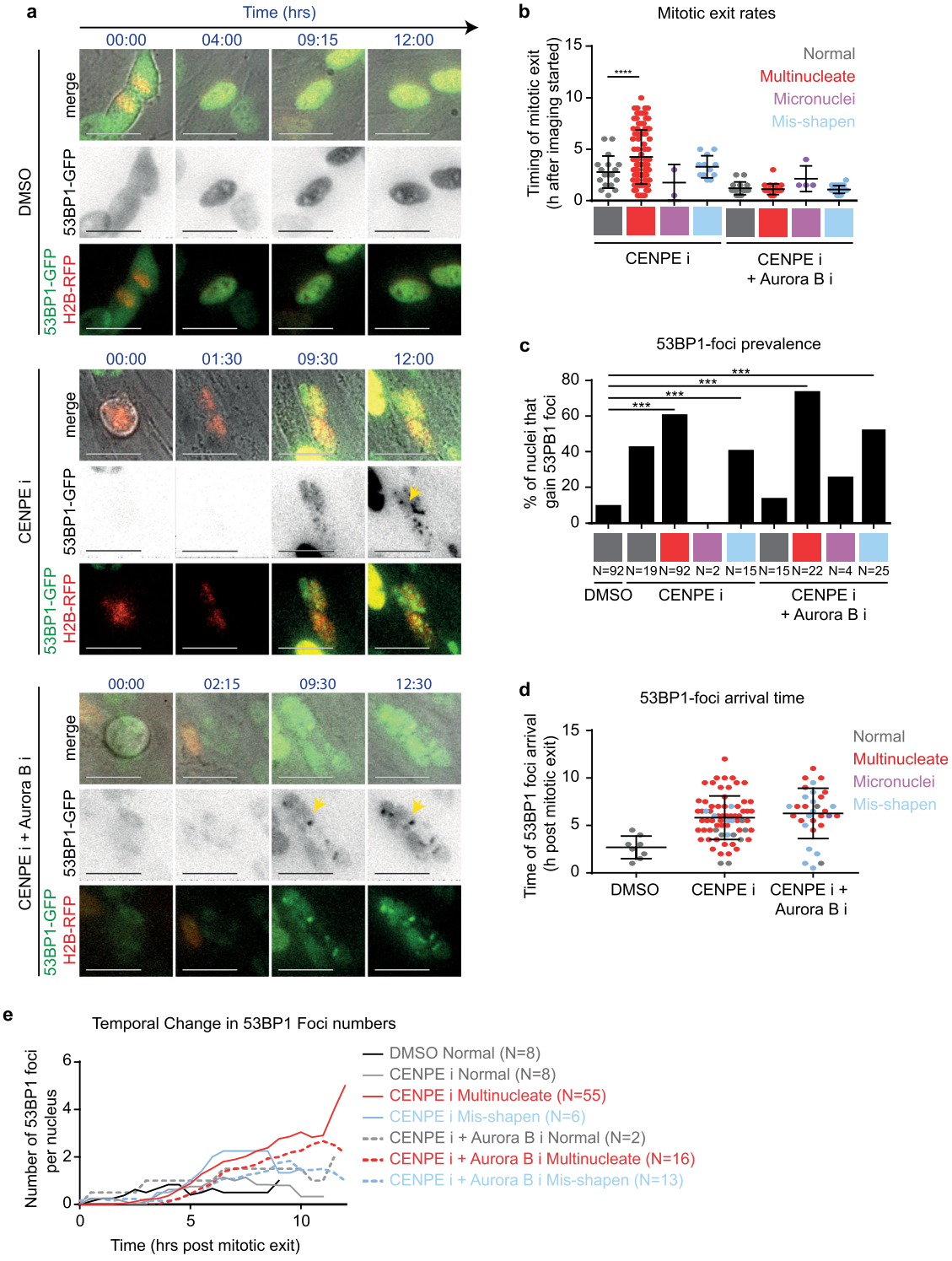

Fig. 2 Multinucleate cells exhibit delayed DNA damage signalling and an increase in damage foci through time. a Representative time-lapse images of normal shaped nuclei exiting mitosis after DMSO treatment, or multinucleated cells exiting mitosis after CENPE i or CENPEi and Aurora Bi treatment as in Supplementary Fig. 5a. Scale 25 μm. Yellow arrows indicate 53BP1-GFP foci within multinucleate cells. In the 53BP1-GFP lane, GFP intensities are inverted to highlight 53BP1-foci as soon as they form (associated supplementary movies present non-inverted GFP intensities). **b** Graph shows the timing of mitotic exit, based on nuclear morphology of daughter cells (indicated by colour). Statistical significance was assessed using an unpaired student's *t* test. **** indicates $p < 0.0001$. **c** Graph of the proportion of daughter nuclei which gain 53BP1 foci during time-lapse imaging. *N* values below bars indicate the number of nuclei from at least three independent experimental repeats. Statistical significance was assessed using a proportions test with 95% confidence interval. *** indicates $p < 0.001$. **d** Graph of the timing of 53BP1 foci arrival in nuclei which gain 53BP1 foci, after drug treatments as indicated. Time-lapse movies as in Fig. 2a were used to determine the earliest time-point of visible 53BP1 foci following mitotic exit. Each value represents one nucleus. The colour of plotted values represents nuclear morphology. **e** Quantification of 53BP1 foci number per nucleus over time from mitotic exit.

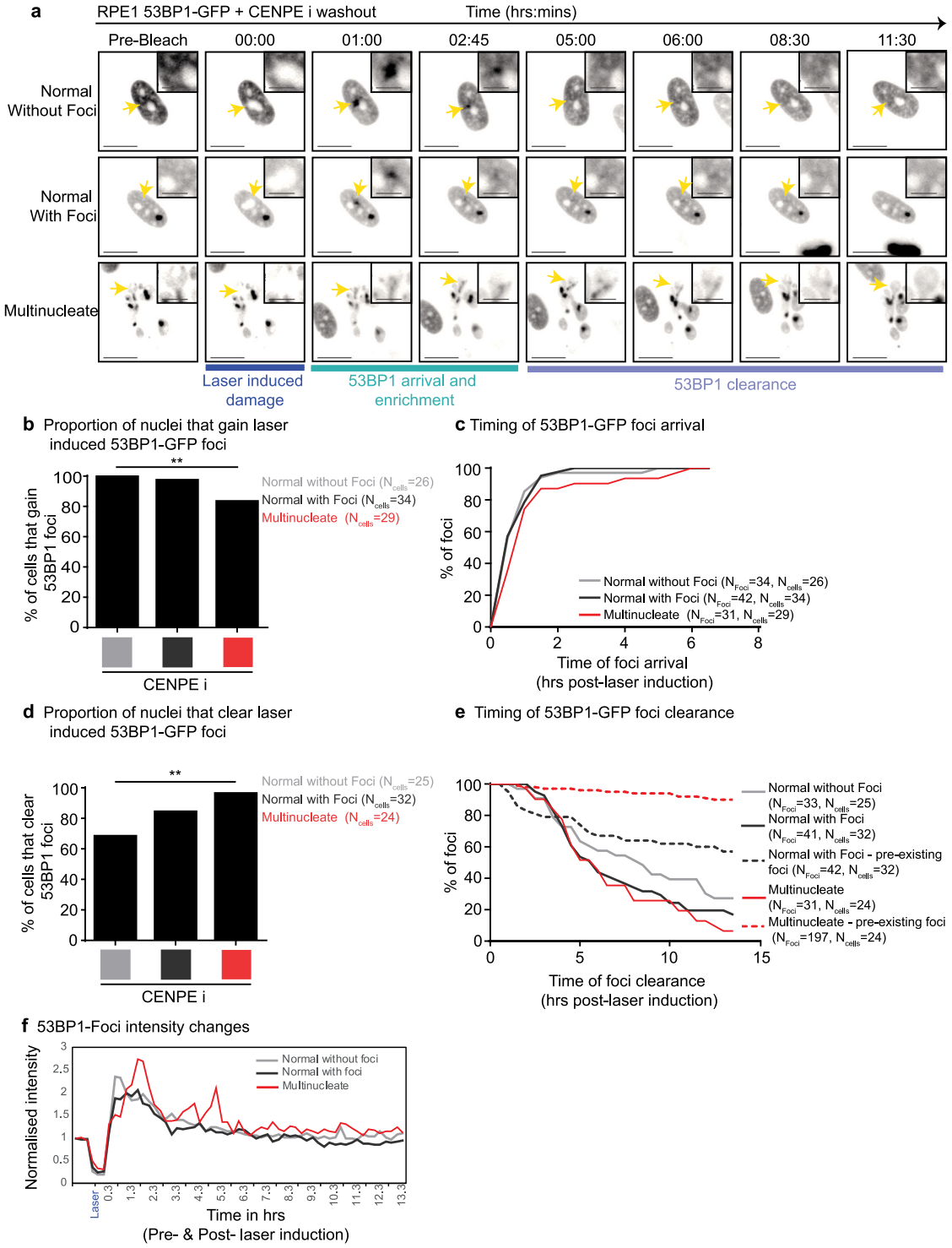

Fig. 3 MADD is not resolved despite intact DDR signalling in multinucleate cells. RPE1 H2B-RFP 53BP1-GFP cells were treated with CENPEi for 24 h, washed and imaging initiated. One laser induced bleach/damage site in each nucleus was tracked. **a** Representative pre-bleach, bleach (at 00:00) and post-bleach images of nuclei—either normal nuclei without pre-existing 53BP1 foci, normal nuclei with pre-existing 53BP1 foci or multinucleate nuclei with 53BP1 foci. Yellow arrows indicate sites of bleaching and are highlighted in crops. Scale 15μm; insets 5μm. **b** Graph shows the proportion of nuclei that gain 53BP1-GFP foci at the site of laser-induced damage, for multinucleate, normal with pre-existing foci and normal nuclei without pre-existing foci. N indicates the number of cells, from across 3 independent repeats. Statistical significance was assessed using a proportions test with a 95% confidence interval. ** indicated $p < 0.05$. **c** Graph shows timing, post-bleach, of 53BP1-GFP foci arrival at the laser bleach site. **d** Quantification of the proportion of nuclei that cleared laser-induced 53BP1-GFP foci, for normal and multinucleate cells. Statistics was assessed using a proportions test with a 95% confidence interval. ** indicates $p < 0.05$. **e** Graph shows the timing of 53BP1-GFP foci clearance after bleach time, for foci induced at the bleach site (solid lines) and foci existing prior to laser bleach (dashed lines). *N* indicates the number of foci and cells analysed. **f** Graph shows changes in 53BP1-GFP foci intensity at laser-induced damage site in cells shown in Fig. 3a. 53BP1-GFP intensities were normalised using pre-laser damage intensity values.

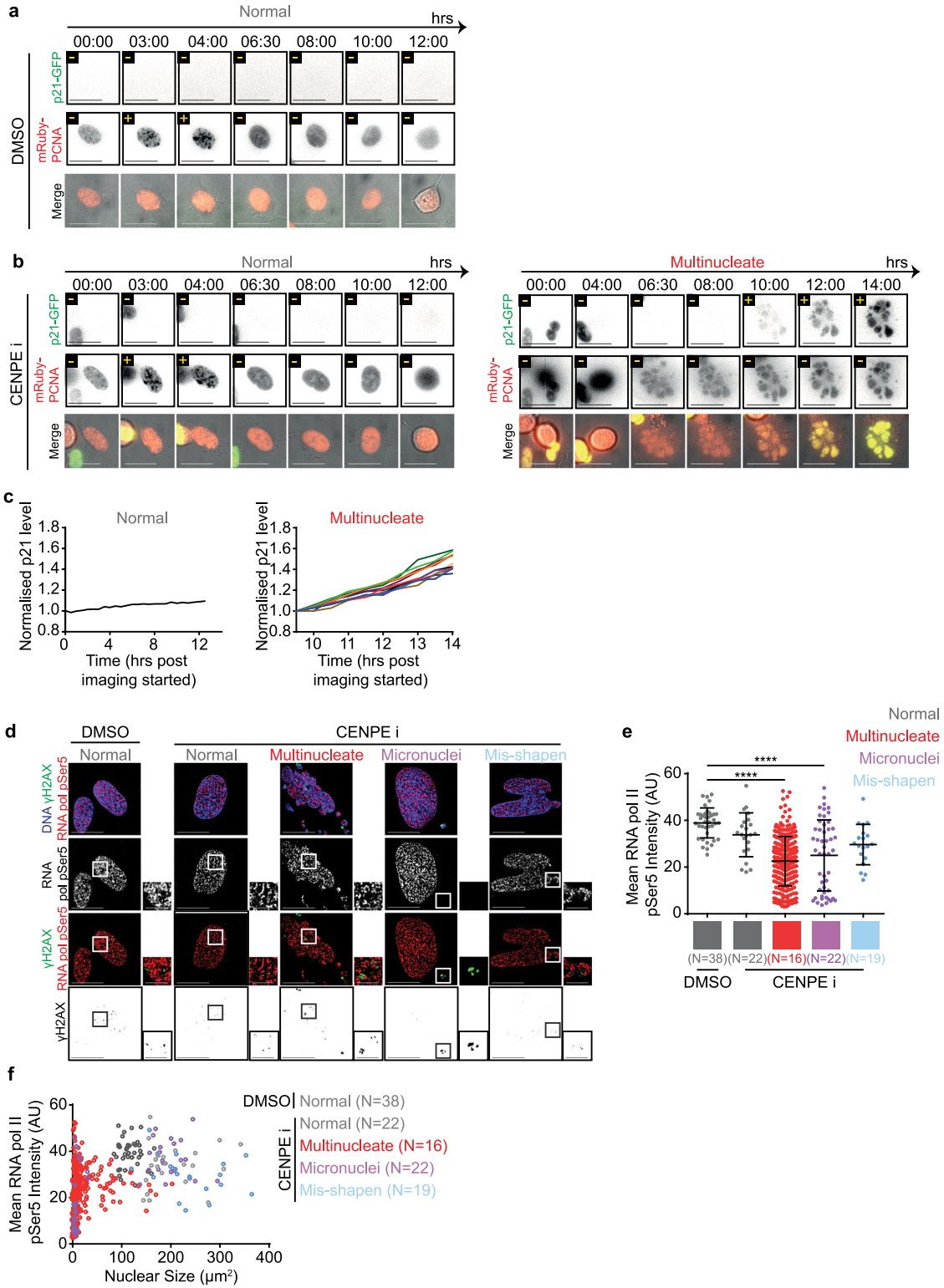

accounted for by a variation in the number of transcriptional sites (Supplementary Fig. 6b, g), revealing a nuclear compartment size cut-off for transcription in multi-nucleated cells. These data show exclusion of transcription at MADD sites and a size-dependent reduction in transcription in multinucleated and micronucleated compartments. In summary, the studies of RNA-pol phosphorylation provide three key insights: (i) multinucleated cells are not dead and are transcriptionally active; (ii) multinucleation induces heterogeneity within nuclear compartments with respect to transcriptional initiation and elongation and (iii) transcriptionally active regions are clearly excluded from MADD sites, indicating the wide impact of MADD to the nearby genome.

Because multinucleated cells cannot resolve MADD (Fig. 3) and display increasing p21 (Fig. 4), we investigated the extent to which multinucleated cells can cross the restriction point[39]. For this purpose, we allowed multinucleated cells to grow for 2 days and assessed DNA damage signalling and cell cycle markers, p53 and phospho-Rb (pRb). Phospho-Rb is a proliferation marker; it

Fig. 4 Multinucleation favours heterogeneous nuclear protein levels. Representative images of RPE1 mRuby-PCNA p21-GFP cells treated with DMSO (**a**) or CENPEi (**b**) for 16 h and washed 10 h prior to live-cell imaging for 14 h. Scale bar 25 μm. Yellow ± refers to p21 or PCNA foci positive or negative respectively. Images show a normal shaped nucleus with low p21 and nuclear PCNA foci and a multinucleate cell, exiting mitosis and building p21-GFP levels through time, without gaining nuclear PCNA foci. **c** Graph of the mean p21 level per nucleus for the normal, or per compartment for multinucleated cells from movies as in Fig. 4a & b. Values are normalised to the mean p21 value from the first time point measured. PCNA signal was used to identify nuclear areas. Colours of lines correspond to different nuclear compartments. **d** RPE1 cells treated with DMSO or CENPEi for 16 h were fixed 48 h later for immunostaining with antibodies against gamma H2AX and RNA pol II CTD pSer5. DNA was stained with DAPI. Representative images of non-overlap between gamma H2AX and RNA pol II pSer5 in cells following DMSO (control) or CENPEi treatment. Scale 15 μm; insets 5 μm. **e** Graph of the mean RNA pol II CTD pSer5 intensity per nucleus (normal or misshapen nuclei) or nuclear compartment (micronucleated and multinucleate). Each plot represents one nucleus/nuclear compartment respectively. *N* refers to the number of cells analysed, across 3 independent repeats. Statistical significance was assessed using a one way ANOVA with multiple comparisons. **f** Mean RNA pol II CTD pSer5 intensity per nucleus/nuclear compartments plotted against the size of the nucleus/nuclear compartment. Line colours represent nuclear morphology as indicated. *N* refers to the number of cells from 3 independent repeats.

is hypophosphorylated in quiescent cells[22]. We find that p53 levels increase in CENPEi-treated cultures, as expected following a prolonged mitotic arrest and DNA damage (Supplementary Fig. 1b), and cells are predominantly negative for pRb, unlike controls (Fig. 5a and Supplementary Fig. 7b). This shows that CENPEi-treated cell cultures do not cross the restriction point normally. To analyse this low pRb phenotype across different forms of atypia, we performed single-cell studies 2 days following the release from mitotic arrest. The proportion of pRb-positive cells was reduced in general but significantly in multinucleated cells (Fig. 5b, c), indicating an impairment in crossing the restriction point and a block in proliferation.

Under conditions inducing DNA damage, a transient reduction in p53 is sufficient to revert quiescent cells into the proliferative state[40,41]. So, we tested whether reducing p53 will allow multinucleated cells to cross the restriction point and transition into the cell cycle. While immunoblots showed an increase in total pRB levels following p53 knockdown (compare CENP-Ei associated lanes of Fig. 5a, d or Supplementary Fig. 7b, c), single-cell studies revealed that this increase in pRB is not prominent in multinucleated cells compared to cells displaying other nuclear atypia (Fig. 5e, f). We conclude that unlike other nuclear atypia, multinucleation robustly blocks proliferation despite compromised p53 (Fig. 5g).

Discussion

We report that multinucleation robustly blocks proliferation despite compromised p53, unlike other forms of nuclear atypia, including micronuclei. This protective aspect of multinucleated cells in blocking DNA replication and S-phase is strongly linked to (i) increasing DNA damage associated 53BP1 bodies in G1-phase which remain unresolved despite an intact NHEJ pathway; (ii) heterogeneous protein localisation and function across nuclear compartments (RNA transcription and protein levels); (iii) lack of transcriptional initiation or elongation foci at MADD sites; and (iv) increasing p21 soon after mitosis (in G1), unlike previously reported stress signals that precede mitosis (in G2)[17,42]. We propose this combination of dysfunctional sub-cellular events associated with multinucleation presents a protective quiescence phenotype despite compromised p53, unlike other nuclear atypia that progress through the cell cycle when p53 is compromised.

Mitotic error induced cell cycle arrest is known, yet a heterogeneity in their cell fates remains unexplained[43–45]; resolving this is important for disease stratification and targeted treatment. To address this knowledge gap, we explore heterogeneity in proliferative fate following the same mitotic perturbance. Previously, the various classes of nuclear atypia have not been quantitatively compared, other than studies of micronuclei alone[3–5]. Prolonged mitosis[46–49] and chromosome missegregation[31,32,50] are well-established causes of p53-mediated G1-arrest. Beyond these, we reveal nuclear compartment status as a predictor of proliferative fate following mitotic error. We demonstrate that multinucleation is associated with a heterogeneous change in transcription and protein accumulation across nuclear compartments, and unresolved MADD associated 53BP1 bodies in G1. Surprisingly, MADD sensing, NHEJ signalling, laser-induced DDR and G1-S inhibition operate normally in multinucleated cells. Unresolved 53BP1 bodies associated with MADD may be similar to DSB-SCARS[51] except that we observe RIF1 accumulation and gH2AX foci and dynamic changes to some (but not all) of the 53BP1 foci in multinucleated cells, indicating additional layers of heterogeneity. The precise molecular reason for differences in 53BP1 foci resolution is unclear and would require future studies downstream of gH2AX-53BP1-RIF1 pathway. Nevertheless, the impact of multinucleation on some but not all subcellular processes presents an advantage for targeted drug treatment of cancers with multinucleated cells, particularly those drugs that disrupt microtubules or mitosis[52,53].

Micronuclei with cytoplasmic DNA mount a protective immune response[54,55], but allow proliferation despite DNA damage, in the face of compromised p53. However, multinucleation blocks G1-S despite compromised p53 and presents exposed DNA, offering additional protection. Our studies of nuclear atypia following mitotic failure (such as those with or without a prolonged mitotic arrest following cytoskeletal or checkpoint defects[56–59]) may also be relevant to nuclear atypia induced by cytoskeletal tension (reviewed in[60]), cell-substrate stiffness[61] or nuclear envelope defects (reviewed in[62]). We propose that unlike other forms of nuclear atypia that show unrestrained proliferation and associated further accumulation of DNA instability, multinucleation presents a protective form proliferation block which should be considered during pathology assessment and post-treatment with anti-mitotics.

Methods

Cell culture and cell lines. RPE1 cells were cultured in DMEM F12 supplemented with 10% foetal calf serum and penicillin and streptomycin. For experiments they were plated onto 13 mm round coverslips for immunofluorescence or onto glass-bottomed dishes (LabTech) for live-cell imaging. All live-cell studies were conducted in stable cell lines: RPE1 H2B-RFP 53BP1-GFP, RPE1 H2B-GFP p53 k.d, mRuby-PCNA and p21-GFP cell lines were all grown in DMEM-F12 and filmed in L15 media.

Drug treatments. To disrupt mitosis cells were treated with 10 nM GSK923295 to inhibit CENPE, 1μM Reversine to inhibit MPS1 and 10μM ZM447439 to inhibit Aurora B. For immunofluorescence experiments drug treatments were incubated for 16 h then washed off and fixed 48 h later, unless indicated otherwise in text.

Live-cell time-lapse imaging. To image cell cycle progression in RPE1 p21-GFP mRuby-PCNA cells, cells were treated with 10 nM GSK923295 or DMSO control for 16 h. Cells were then washed and then additionally treated with DMSO or 10 μM ZM447439. 10 h later cells were washed and media changed to Leibovitz (L15) imaging media at 37 °C and imaging started. An image was taken at least every 30 min for 14 h. Images were acquired using a 40 × 0.75NA objective on a DeltaVision Core^{TM} microscope (GE Healthcare) with a Cascade2 camera under EM mode to allow live-imaging of proliferating cells overnight[63].

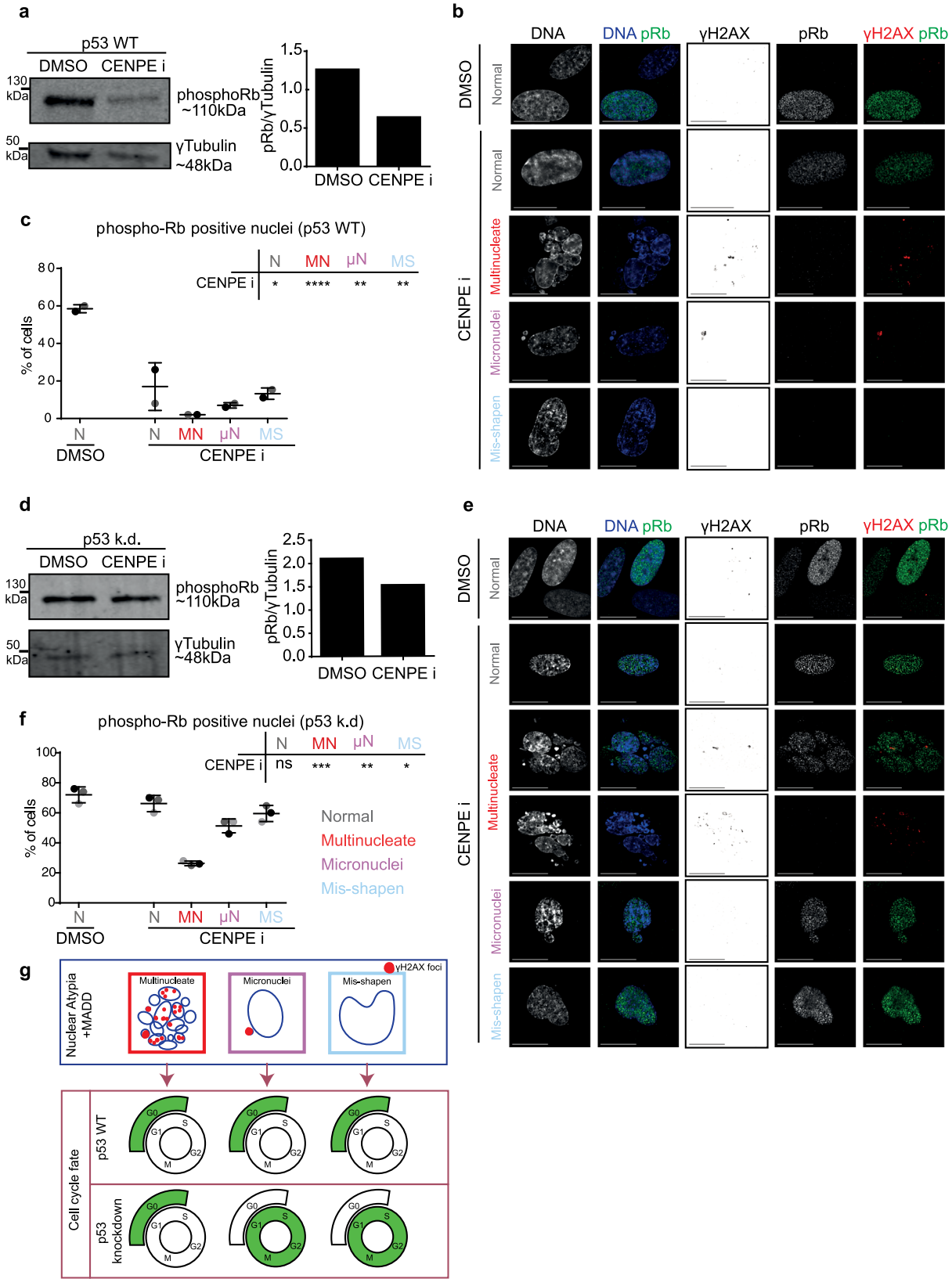

To image 53BP1-GFP foci arrival in cells following mitotic disruption RPE1 H2B-RFP 53BP1-GFP cells were treated with DMSO or GSK923295 for 24 h. Cells were washed and then transferred to 37 °C Leibovitz imaging media with DMSO or ZM447429 in the media. Cells were then imaged for at least 12 h with an image taken at least every 30 min. Images were acquired using a 40 × 0.75NA objective on a DeltaVision Core™ microscope (GE Healthcare) with a Cascade2 camera under EM mode.

FRAP photobleaching to induce 53BP1-GFP foci. The Deltavision Core™ microscope was used with the FRAP tool using Quantifiable laser module components (488 nm laser). Target points were identified and then bleached with a pulse duration of 1 s and a laser power of 30%. 3 pre-bleach and 3 post-bleach images were taken at each target site, all 0.5 s apart, using a 60×1.42 NA objective, using CoolSnap HQ camera (Photometrics). Following each site being bleached, a time-lapse microscope was initiated for the following 13 h with an image acquired

Fig. 5 Multinucleated cells uniquely display reduced phospho-Rb despite compromised p53. RPE1 p53 WT (**a**–**c**) or RPE1 H2B-GFP p53 k.d. **d**–**f** cells were treated with DMSO or CENPEi for 16 h and 48 h later cells were immunostained with antibodies against pRb and gamma H2AX, or cells were lysed for immunoblot. **a & d** Immunoblot shows pRb or gamma-tubulin levels in RPE1 p53 WT (**a**) or p53 kd (**d**) cells following DMSO or CENPEi treatment, as indicated. Note the gamma-tubulin is the same as displayed in Supplementary Fig. 1. Right panel shows a graph of pRb fluorescent intensity, normalised to gamma-tubulin. Representative images of nuclear atypia following CENPEi treatment of RPE1 p53 WT (**b**) or p53 kd (**e**) cells. Scale 15 μm. Graph of proportion of pRb positive or negative RPE1 WT (**c**) or p53 kd (**f**) cells, after DMSO or CENPEi treatment. $N > 100$ for WT or >150 for p53 k.d cells from 2 or 3 independent repeats (shown as shades of grey), respectively. Statistical analysis using multiple unpaired t-tests, comparing each morphology after CENPEi treatment to normal nuclei after DMSO. **g** Model comparing nuclear atypia shows large-scale DNA damage in multinucleate cells, but not in misshapen nuclei, and in micronucleated cells, gamma H2AX foci are majority confined to the micronucleus. Nuclear atypia causes G0 arrest in p53 WT. In p53 k.d. conditions, only multinucleate cells are G0 arrested.

every 30 min, using a 40×0.75 NA objective with a Cascade2 camera under EM mode.

Immunofluorescence. For immunofluorescence the following antibodies were used; PCNA UniProt:P12004 (CST, 3586 S, 1:1000), Phospho-Rb (Ser 807/811) (CST, 8516 S, 1:1000), γH2AX (Abcam, ab26350, 1:800), γH2AX (CST. 1:1000), GFP (Abcam, ab290, 1:1000), RNA polymerase II CTD repeat phospho-Ser2 (Abcam, ab126353, 1:1000) and RNA polymerase II CTD repeat phospho-Ser5 (Abcam, ab5408, 1:1000). DNA was stained with DAPI. Cells were fixed with ice-cold methanol and blocked with 1% BSA in PBS before immunostaining. Images of immunostained cells were acquired using a 100×1.2 NA objective on a DeltaVision Core microscope with a CoolSnap HQ camera (Photometrics). Cells were scored as positive for PCNA foci when foci signal intensities associated with the PCNA foci (inside the nuclei) were well above the background speckles outside the nuclei.

Nuclear atypia scoring. DAPI stained nuclei were categorised based upon nuclear appearance, for nuclear morphology. As in Fig. 1b, normal nuclei were those that had a continuous nuclear periphery and a regular oval shape, abnormal shaped nuclei were those that deviated from this regular oval shape but the nuclear material was contained within one nuclear compartment. Micronucleated cells have one or a few nuclear compartments external to the primary nucleus, containing one or a fragment of a chromosome. Multinucleate cells have multiple nuclear compartments varying in size, and can include micronuclei.

Image analysis. Image J was used for measurements of fluorescence intensities, using 8-bit images as in[64]. Softworx was used for manual image analysis of 53BP1-GFP foci tracking.

Statistics and reproducibility. All experiments were independently repeated at least thrice and statistical significance of phenotypes across biological replicates assessed. The exact sample size (n) for each experimental group/condition, is included in figure caption as a discrete number. Graphs were plotted using Graphpad Prism, which was also used for statistical testing, except form proportions tests which were carried out in Microsoft Excel. In all graphs presented, error bars represent standard deviation. In statistical tests presented the following indications for p values were used; non-significant – ns for $p > 0.05$, * for $p < 0.05$, ** for $p < 0.01$, *** for $p < 0.001$, **** for $p < 0.0001$.

Reporting summary. Further information on research design is available in the Nature Research Reporting Summary linked to this article.

Data availability

All raw video and image data are available on request from the authors. All numerical datasets used in the study are available at Figshare for download https://doi.org/10.6084/m9.figshare.14159024. The raw data files include the quantification of cell fates and fluorescence particle size and intensities.

Received: 14 January 2020; Accepted: 11 March 2021;
Published online: 09 April 2021

References

1. Kadota, K. et al. A nuclear grading system is a strong predictor of survival in epitheloid diffuse malignant pleural mesothelioma. *Mod. Pathol.* **25**, 260–271 (2012).
2. Kadota, K. et al. A grading system combining architectural features and mitotic count predicts recurrence in stage I lung adenocarcinoma. *Mod. Pathol.* **25**, 1117–1127 (2012).
3. Hatch, E. M., Fischer, A. H., Deerinck, T. J. & Hetzer, M. W. Catastrophic nuclear envelope collapse in cancer cell micronuclei. *Cell* **154**, 47–60 (2013).
4. Crasta, K. et al. DNA breaks and chromosome pulverization from errors in mitosis. *Nature* **482**, 53–58 (2012).
5. Zhang, C.-Z. et al. Chromothripsis from DNA damage in micronuclei. *Nature* **522**, 179–184 (2015).
6. Ly, P. et al. Selective Y centromere inactivation triggers chromosome shattering in micronuclei and repair by non-homologous end joining. *Nat. Cell Biol.* **19**, 68–75 (2017).
7. Soto, M. et al. p53 prohibits propagation of chromosome segregation errors that produce structural aneuploidies. *Cell Rep.* **19**, 2423–2431 (2017).
8. Brito, D. A. & Rieder, C. L. Mitotic checkpoint slippage in humans occurs via cyclin B destruction in the presence of an active checkpoint. *Curr. Biol.* **16**, 1194–1200 (2006).
9. Zhu, Y., Zhou, Y. & Shi, J. Post-slippage multinucleation renders cytotoxic variation in anti-mitotic drugs that target the microtubules or mitotic spindle. *Cell Cycle* **13**, 1756–1764 (2014).
10. Pedersen, R. S. et al. Profiling DNA damage response following mitotic perturbations. *Nat. Commun.* **7**, 13887 (2016).
11. Mirzayans, R., Andrais, B. & Murray, D. Roles of polyploid/multinucleated giant cancer cells in metastasis and disease relapse following anticancer treatment. *Cancers* **10**, 118–129 (2018).
12. Draviam, V. M., Xie, S. & Sorger, P. K. Chromosome segregation and genomic stability. *Curr. Opin. Genet. Dev.* **14**, 120–125 (2004).
13. Mythily, D. V., Krishna, S. & Tergaonkar, V. Pleiotropic effects of human papillomavirus type 16 E6 oncogene expression in human epithelial cell lines. *J. Gen. Virol.* **80**, 1707–1713 (1999).
14. Gasco, M., Shami, S. & Crook, T. The p53 pathway in breast cancer. *Breast Cancer Res.* **4**, 70–76 (2002).
15. Overton, K. W., Spencer, S. L., Noderer, W. L., Meyer, T. & Wang, C. L. Basal p21 controls population heterogeneity in cycling and quiescent cell cycle states. *Proc. Natl Acad. Sci. USA.* **111**, E4386–E4393 (2014).
16. Arora, M., Moser, J., Phadke, H., Basha, A. A. & Spencer, S. L. Endogenous replication stress in mother cells leads to quiescence of daughter cells. *Cell Rep.* **19**, 1351–1364 (2017).
17. Spencer, S. L. et al. The proliferation-quiescence decision is controlled by a bifurcation in CDK2 activity at mitotic exit. *Cell* **155**, 369–383 (2013).
18. Cappell, S. D., Chung, M., Jaimovich, A., Spencer, S. L. & Meyer, T. Irreversible APC(Cdh1) inactivation underlies the point of no return for cell-cycle entry. *Cell* **166**, 167–180 (2016).
19. Gookin, S. et al. A map of protein dynamics during cell-cycle progression and cell-cycle exit. *PLoS Biol.* **15**, e2003268 (2017).
20. Dai, L. et al. SETD4 regulates cell quiescence and catalysts the H4K20 during diapause formation in Artemia. *Mol. Cell. Biol.* **37**, e00453–16 (2017).
21. Kwon, J. S. et al. Controlling depth of cellular quiescence by an Rb-E2F network switch. *Cell Rep.* **20**, 3223–3235 (2017).
22. Moser, J. et al. Control of the Restriction Point by Rb and p21. *Proc. Natl. Acad. Sci. USA.* **35**, E8219–E8227 (2018).
23. Shi, J. & Mitchison, T. J. Cell death response to anti-mitotic drug treatment in cell culture, mouse tumor model and the clinic. *Endocr. Relat. Cancer* **24**, T83–T96 (2017).
24. Soto, M., García-Santisteban, I., Krenning, L., Medema, R. H. & Raaijmakers, J. A. Chromosomes trapped in micronuclei are liable to segregation errors. *J. Cell Sci.* **131**, jcs214742 (2018).
25. Shrestha, R. L. & Draviam, V. M. Lateral to end-on conversion of chromosome-microtubule attachment requires kinesins CENP-E and MCAK. *Curr. Biol.* **23**, 1514–1526 (2013).
26. Kuhn, J. & Dumont, S. Spindle assembly checkpoint satisfaction occurs via end-on but not lateral attachments under tension. *J. Cell Biol.* **216**, 1533–1542 (2017).
27. Wood, K. W. et al. Antitumor activity of an allosteric inhibitor of centromere-associated protein-E. *Proc. Natl Acad. Sci. U S A.* **107**, 5839–5844 (2010).
28. Weihua, Z., Lin, Q., Ramoth, A. J., Fan, D. & Fidler, I. J. Formation of solid tumors by a single multinucleated cancer cell. *Cancer* **117**, 4092–4099 (2011).
29. Muller, P. A. J. & Vousden, K. H. p53 mutations in cancer. *Nat. Cell Biol.* **15**, 2–8 (2013).

30. Fujiwara, T. et al. Cytokinesis failure generating tetraploids promotes tumorigenesis in p53-null cells. *Nature* **437**, 1043–1047 (2005).
31. Thompson, S. L. & Compton, D. A. Proliferation of aneuploid human cells is limited by a p53-dependent mechanism. *J. Cell Biol.* **188**, 369–381 (2010).
32. Santaguida, S. et al. Chromosome mis-segregation generates cell-cycle-arrested cells with complex karyotypes that are eliminated by the immune system. *Dev. Cell* **41**, 638–651 (2017). e5.
33. Liu, S. et al. Nuclear envelope assembly defects link mitotic errors to chromothripsis. *Nature* **561**, 551–555 (2018).
34. Escribano-Dıaz, C. et al. A cell cycle-dependent regulatory circuit composed of 53BP1-RIF1 and BRCA1-CtIP controls DNA repair pathway choice. *Mol. Cell* **49**, 872–883 (2013).
35. Zimmermann, M., Lottersberger, F., Buonomo, S. B., Sfeir, A. & de Lange, T. 53BP1 regulates DSB repair using Rif1 to control 5' end resection. *Science* **339**, 700–704 (2013).
36. Chapman, J. R. et al. RIF1 is essential for 53BP1-dependent nonhomologous end joining and suppression of DNA double-strand break resection. *Mol. Cell* **49**, 858–871 (2013).
37. Corrigan, A. M. et al. Automated tracking of mitotic spindle pole positions shows that LGN is required for spindle rotation but not orientation maintenance. *Cell Cycle* **12**, 2643–2655 (2013).
38. Harrigan, J. A. et al. Replication stress induces 53BP1-containing OPT domains in G1 cells. *J. Cell Biol.* **193**, 97–108 (2011).
39. Heldt, F. S., Barr, A. R., Cooper, S., Bakal, C. & Novák, B. A comprehensive model for the proliferation-quiescence decision in response to endogenous DNA damage in human cells. *Proc. Natl Acad. Sci. USA.* **115**, 2532–2537 (2018).
40. Heldt, F. S. et al. A comprehensive model for the proliferation-quiescence decision in response to endogenous DNA damage in human cells. *Proc. Natl. Acad. Sci. USA.* **10**, 2532–2537 (2018).
41. Reyes, M. E. et al. RNA sequence analysis of inducible pluripotent stem cell-derived cardiomyocytes reveals altered expression of DNA damage and cell cycle genes in response to doxorubicin. *Toxicol. Appl. Pharmacol.* **356**, 44–53 (2018).
42. Barr, A. R. et al. DNA damage during S-phase mediates the proliferation-quiescence decision in the subsequent G1 via p21 expression. *Nat. Commun.* **8**, 14728–14745 (2017).
43. Gascoigne, K. E. & Taylor, S. S. Cancer cells display profound intra- and interline variation following prolonged exposure to antimitotic drugs. *Cancer Cell* **14**, 111–122 (2008).
44. Orth, J. D. et al. Quantitative live imaging of cancer and normal cells treated with Kinesin-5 inhibitors indicates significant differences in phenotypic responses and cell fate. *Mol. Cancer Ther.* **7**, 3480–3489 (2008).
45. Shi, J., Orth, J. D. & Mitchison, T. Cell type variation in responses to antimitotic drugs that target microtubules and kinesin-5. *Cancer Res.* **68**, 3269–3276 (2008).
46. Uetake, Y. & Sluder, G. Prolonged prometaphase blocks daughter cell proliferation despite normal completion of mitosis. *Curr. Biol.* **20**, 1666–1671 (2010).
47. Orth, J. D., Loewer, A., Lahav, G. & Mitchison, T. J. Prolonged mitotic arrest triggers partial activation of apoptosis, resulting in DNA damage and p53 induction. *Mol. Biol. Cell* **23**, 567–576 (2012).
48. Fong, C. S. et al. 53BP1 and USP28 mediate p53-dependent cell cycle arrest in response to centrosome loss and prolonged mitosis. *Elife* **5**, 16270–16288 (2016).
49. Dalton, W. B., Nandan, M. O., Moore, R. T. & Yang, V. W. Human cancer cells commonly acquire DNA damage during mitotic arrest. *Cancer Res.* **67**, 11487–11492 (2007).
50. Dobles, M., Liberal, V., Scott, M. L., Benezra, R. & Sorger, P. K. Chromosome missegregation and apoptosis in mice lacking the mitotic checkpoint protein Mad2. *Cell* **101**, 635–645 (2000).
51. Rodier, F. et al. DNA-SCARS: distinct nuclear structures that sustain damage-induced senescence growth arrest and inflammatory cytokine secretion. *J. Cell Sci.* **124**, 68–81 (2011).
52. Iorio, F. et al. A semi-supervised approach for refining transcriptional signatures of drug response and repositioning predictions. *PLoS One* **10**, e0139446 (2015).
53. Iorio, F. et al. A landscape of pharmacogenomic interactions in cancer. *Cell* **166**, 740–754 (2016).
54. Mackenzie, K. J. et al. cGAS surveillance of micronuclei links genome instability to innate immunity. *Nature* **548**, 461–465 (2017).
55. Harding, S. M. et al. Mitotic progression following DNA damage enables pattern recognition within micronuclei. *Nature* **548**, 466–470 (2017).
56. Shrestha, R. L. et al. Aurora-B kinase pathway controls the lateral to end-on conversion of kinetochore-microtubule attachments in human cells. *Nat. Commun.* **8**, 150 (2017).
57. Shrestha, R. L. et al. TAO1 kinase maintains chromosomal stability by facilitating proper congression of chromosomes. *Open Biol.* **4**, 130108 (2014).
58. Meraldi, P., Draviam, V. M. & Sorger, P. K. Timing and checkpoints in the regulation of mitotic progression. *Dev. Cell* **7**, 45–60 (2004).
59. Patel, H. et al. Kindlin1 regulates microtubule function to ensure normal mitosis. *J. Mol. Cell Biol.* **8**, 338–348 (2016).
60. Lele, T. P., Dickinson, R. B. & Gundersen, G. G. Mechanical principles of nuclear shaping and positioning. *J. Cell Biol.* **217**, 3330–3342 (2018).
61. Lovett, D. B., Shekhar, N., Nickerson, J. A., Roux, K. J. & Lele, T. P. Modulation of nuclear shape by substrate rigidity. *Cell. Mol. Bioeng.* **6**, 230–238 (2013).
62. Worman, H. J. & Bonne, G. 'Laminopathies': a wide spectrum of human diseases. *Exp. Cell Res.* **313**, 2121–2133 (2007).
63. Zulkipli, I. et al. Spindle rotation in human cells is reliant on a MARK2-mediated equatorial spindle-centering mechanism. *J. Cell Biol.* **217**, 3057–3070 (2018).
64. Conti, D. et al. Kinetochores attached to microtubule-ends are stabilised by Astrin bound PP1 to ensure proper chromosome segregation. *Elife* **8**, 49325 (2019).

Acknowledgements

The work was supported by funding to Draviam by a BBSRC research grant (R01003X/1) and QMUL start-up grant (SBC8DRA2). We thank the Medema and Barr labs for providing RPE1 H2B-RFP 53BP1-GFP cell line, RPE1 mRuby-PCNA & p21-GFP and RPE1 H2B-GFP p53 k.d. cell line as gifts, and the Draviam laboratory members for discussions on data analysis and presentation.

Author contributions

Original project goals were conceived by V.M.D., experiments were designed by V.M.D. and M.H. Experiments related to all figures except for Supplementary Figure panels 1A and 7A were performed and analysed by M.H. S.A. performed experiments related to Supplementary Figure panels 1A and 7A. The manuscript was written and edited by V. M.D. and M.H. with comments from S.A. and Draviam laboratory members.

Competing interests

The authors declare no competing interests.

Additional information

Supplementary information The online version contains supplementary material available at https://doi.org/10.1038/s42003-021-01979-5.

Correspondence and requests for materials should be addressed to V.M.D.

Reprints and permission information is available at http://www.nature.com/reprints

Publisher's note Springer Nature remains neutral with regard to jurisdictional claims in published maps and institutional affiliations.